

Large tensile plasticity induced by pronounced β -relaxation in Fe-based metallic glass via cryogenic thermal cycling

Siyi Di ^a, Haibo Ke ^b, Qianqian Wang ^{a,c}, Jing Zhou ^{b,d}, Yong Zhao ^b, Baolong Shen ^{a,*}

^a School of Materials Science and Engineering, Jiangsu Key Laboratory for Advanced Metallic Materials, Southeast University, Nanjing 211189, China

^b Songshan Lake Materials Laboratory, Dongguan 523808, China

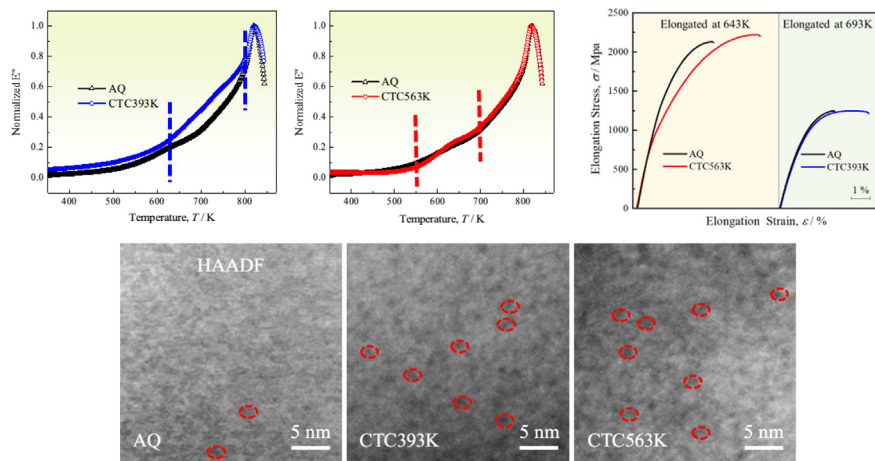
^c School of Materials Science and Engineering, Jiangsu Key Laboratory of Advanced Structural Materials and Application Technology, Nanjing Institute of Technology, Nanjing 211167, China

^d School of Mechanical Engineering, Dongguan University of Technology, Dongguan 523808, China

HIGHLIGHTS

- FeCoBSiNb metallic glass shows pronounced β -relaxation and large tensile plasticity after cryogenic thermal cycling.
- Increase of structural heterogeneity leads to pronounced β -relaxation and enhanced tensile plasticity.
- β -relaxation exhibits separate peaks with diverse cycling temperatures, which is resulted from different sizes/types of shear transformation zones.

GRAPHICAL ABSTRACT



ARTICLE INFO

Article history:

Received 19 April 2022

Revised 29 June 2022

Accepted 17 August 2022

Available online 18 August 2022

Keywords:

Metallic glass

Tensile plasticity

Cryogenic thermal cycling

β -relaxation

ABSTRACT

The effects of cryogenic thermal cycling (CTC) treatment on tensile plasticity and structure change of [(Fe_{0.5}Co_{0.5})_{0.75}B_{0.2}Si_{0.05}]₉₆Nb₄ metallic glass (MG) ribbons were systematically investigated. Pronounced β -relaxation peaks locating at 643 and 693 K were observed after CTC treatment with diverse thermal temperatures. Specifically, the CTC treated samples exhibiting most remarkable β -relaxation showed tensile plastic strain of 5.2% at 643 K and 4% at 693 K, while the as-quenched sample only showed tensile plastic strain of 3% at 643 K and 2.1% at 693 K. The pronounced β -relaxation and enhanced tensile plasticity are considered to be originated from the increased structural heterogeneity. The separate β -relaxation peaks result from the different sizes/types of shear transformation zones induced by oscillatory (rejuvenation-relaxation) behavior during thermal cycling. Our results indicate that the CTC treatment has a significant impact on the energy states and structural heterogeneity, which makes it a powerful means to modify the mechanical properties of MGs.

© 2022 The Authors. Published by Elsevier Ltd. This is an open access article under the CC BY-NC-ND license (<http://creativecommons.org/licenses/by-nc-nd/4.0/>).

* Corresponding author.

E-mail address: blshen@seu.edu.cn (B. Shen).

1. Introduction

Fe-based metallic glasses (MGs) have aroused tremendous interest owing to their extraordinary high strength, excellent soft magnetic properties, and relatively low production costs [1–3]. However, their application is often limited by room-temperature brittleness, especially the almost negligible tensile ductility [2–4]. Under loading, MGs suffer from extreme shear localization in narrow shear bands (SBs), leading to local softening and the following shear instability [5,6]. In tensile testing, MGs can be much more susceptible to early failure, the presence of dominant tensile stresses is known to quickly trigger crack formation upon the formation of first SB [7,8]. Considerable efforts have been dedicated to improve the deformation ability of Fe-based MGs in the past decades, for example, adding elements with high Poisson's ratio or low shear modulus [9,10], introducing structural heterogeneities by phase separation or short/medium range ordering clusters [11,12], and developing composite microstructure by precipitating crystalline phases [13,14]. However, these methods mostly focus on the compressive deformation ability and sometimes deteriorate the soft magnetic properties of Fe-based MGs.

Recently, it has been revealed that the properties of MGs can be tailored by modulating their energy states, and rejuvenation is effective to improve the deformation ability [15,16]. Among various rejuvenation methods, a thermal treatment method named cryogenic thermal cycling (CTC) has attracted more attention due to the merits of non-destructive, isotropic and controllable [17]. It has been proved to be beneficial to the compressive plasticity and fracture toughness of various MGs [18,19]. Particularly, it is barely detrimental to the soft magnetic properties of Fe-based MGs [20]. However, some MGs have no response and even undergo decreased plasticity after CTC treatment [21]. It is evident from both experiments [22,23] and simulations [24] that the effect of CTC treatment is delicately balanced between relaxation and rejuvenation, which gives rise to the scattering of resulted plasticity in different MG systems. The structural mechanism of oscillatory (rejuvenation-relaxation) behavior during CTC treatment ought to be revealed to make this method more applicable. In previous study, effects of cycling number during CTC treatment on structure and mechanical properties were usually studied, while the effects of thermal temperature were barely investigated, which maybe more sensitive and comprehensible to the oscillatory behavior during thermal cycling.

The compressive plasticity of $[(\text{Fe}_{0.5}\text{Co}_{0.5})_{0.75}\text{B}_{0.2}\text{Si}_{0.05}]_{96}\text{Nb}_4$ bulk metallic glass has been significantly improved via CTC treatment [22] but the enhancement of tensile plasticity remains a challenge. In this study, ribbons of this alloy were prepared to explore the influence of CTC treatment with different thermal temperatures on its tensile ductility. After CTC treatment, the MG ribbons showed pronounced β -relaxation at two different temperature regions, leading to the improved tensile plasticity. The pronounced β -relaxation and enhanced tensile ductility were revealed to be associated with the increased structural heterogeneity caused by thermal cycling. These results indicated that CTC treatment would be an attractive and promising approach to develop new MG materials with superior deformation ability.

2. Experimental methods

MG ribbons with nominal composition of $[(\text{Fe}_{0.5}\text{Co}_{0.5})_{0.75}\text{B}_{0.2}\text{Si}_{0.05}]_{96}\text{Nb}_4$ were prepared by melt spinning. CTC treatment with different thermal temperatures (0.43–0.69 of glass transition temperature, T_g) were applied to the ribbons. In each cycle, the ribbons were firstly dipped into liquid nitrogen for 1 min, then immediately immersed in hot silicone oil for 1 min. A whole CTC treatment

includes 15 cycles. The schematic diagram of the process is shown in Fig. 1.

The enthalpies of relaxation (ΔH_{rel}) for the as-quenched and CTC treated samples were measured by differential scanning calorimeter (DSC, Netzsch 404 F3). The samples were heated from 313 to 973 K (above T_g) at a heating rate of 20 K/min, and then cooled to 313 K, followed by a second cycle using the same procedure. The ΔH_{rel} was calculated from the area difference between the first and second cycle curves below T_g . Five samples for each condition were tested to ensure the repeatability. The relaxation dynamics of the MGs before and after thermal cycling were studied by dynamical mechanical analyzer (DMA, Netzsch DMA 242 E). The measurements were conducted at a heating rate of 3 K/min using the testing frequency of 1 Hz. Besides, uniaxial tensile tests at chosen temperatures were carried out on a TA Q850 DMA at a strain rate of 10^{-4} s^{-1} . Three samples for each condition were tested for repeatability. The morphologies of the surface and vertical section after fracture were observed by scanning electron microscopy (SEM, Sirion 200, FEI). High-resolution transmission electron microscopy (HRTEM, Talos F200X) analysis was carried out to observe the microstructure changes before and after thermal cycling. The samples for HRTEM analysis were thinned by ion milling method (Gatan Inc., PIPS-M691) under liquid nitrogen cooling condition. The elemental distributions on nanoscale were analyzed by energy-dispersive X-ray spectroscopy (EDS) in TEM. For high angle annular dark-field (HAADF) imaging, a probe semi-convergence angle of 10.5 mrad and collection semi-angle of 58–200 mrad were used.

The nanoindentation tests were performed using a NanoTest instrument (Micro Materials Ltd) with a standard Berkovich diamond indenter to calculate the activation volume of shear transformation zone (STZ). Four different loading rates of 0.5, 1, 5, and 10 mN/s were applied. For each sample and loading rate, five effective indentation tests were performed.

3. Results

3.1. Mechanical response to CTC treatment

The dynamic mechanical behavior of the samples before and after thermal cycling are studied through DMA. The temperature dependence of the normalized loss modulus E'' of the as-

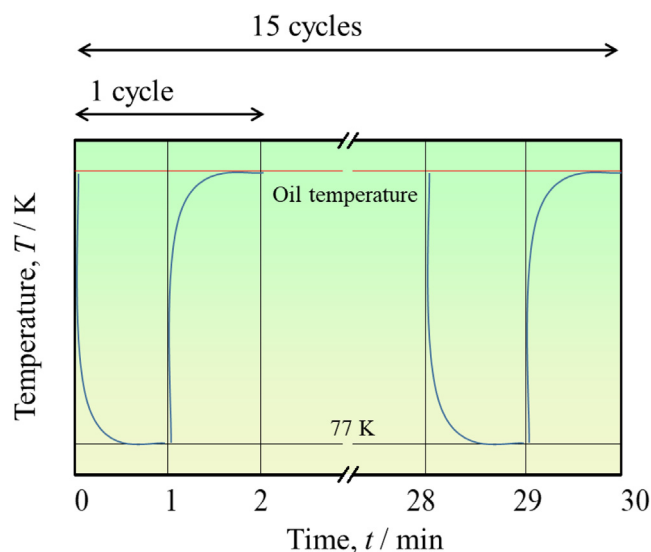


Fig. 1. Schematic diagram of the CTC process.

quenched $[(\text{Fe}_{0.5}\text{Co}_{0.5})_{0.75}\text{B}_{0.2}\text{Si}_{0.05}]_{96}\text{Nb}_4$ ribbon (denoted as AQ) and those after CTC treatment with different thermal temperatures (denoted as CTC-cycling temperature) are shown in Fig. 2(a). The following remarkable features can be noticed: all the samples show distinct peaks at a high temperature around 820 K, which is identified as α -relaxation. At lower temperature, the CTC treated samples show more pronounced β -relaxation peaks and interestingly, it seems that the β -relaxation peaks appear at two different positions for samples with different cycling temperatures. For AQ, CTC453K, CTC493K, CTC533K and CTC563K samples, the β -relaxation peaks are around 550–700 K (0.68 – $0.86 T_g$). For CTC353K, CTC393K and CTC433K samples, the β -relaxation peaks exhibit a noticeable excess wing, locating around 620–790 K (0.76 – $0.96 T_g$). For clarity, the CTC393K and CTC563K samples, which show most conspicuous β -relaxation peaks at the two temperature regions are compared with the AQ sample, as shown in Fig. 2(b) and Fig. 2(c), respectively. The temperature of β -relaxation peak is about 643 K for AQ and CTC563K samples, and 693 K for CTC393K sample. Previously, it has been demonstrated that β -relaxation may share identical microstructural origins with plastic deformation carrier, i.e., STZ [25], MG samples with pronounced β -relaxation often have better ductility [26]. Because the CTC563K and CTC393K samples show most conspicuous β -relaxation among all the samples, the two samples may exhibit superior deformation ability.

The tensile properties of AQ, CTC563K and CTC393K samples are tested at the corresponding β -relaxation peak temperatures, 643 and 693 K. The typical tensile stress–strain curves are shown in Fig. 3. At 643 K, the tensile plastic strain (ε_p) is 3% for AQ sample and 5.2% for CTC563K sample. At 693 K, the ε_p is 2.1% for AQ sample and 4.0% for CTC393K sample. The two samples after CTC treatment obtain significantly improved tensile plasticity. The yield strength (σ_y) and fracture strength (σ_f) are 980 MPa and 2128 MPa for AQ sample, and 750 MPa and 2220 MPa for CTC563K sample at 643 K. At elevated temperature of 693 K, the σ_y and σ_f are 680 MPa and 1247 MPa for AQ sample, 620 MPa and 1245 MPa for CTC393K sample, respectively. It is clear that elevated deformation temperature leads to the decrease of strength, consistent with other reports [27]. The decreased σ_y originates from the decreased activation energy and easier activation of soft regions at higher temperature [28]. However, the ε_p of AQ sample at 693 K is smaller than that at 643 K, which suggests that homogeneous flow is not the dominate mechanism at these two temperatures. The larger ε_p of AQ sample at 643 K originates from the

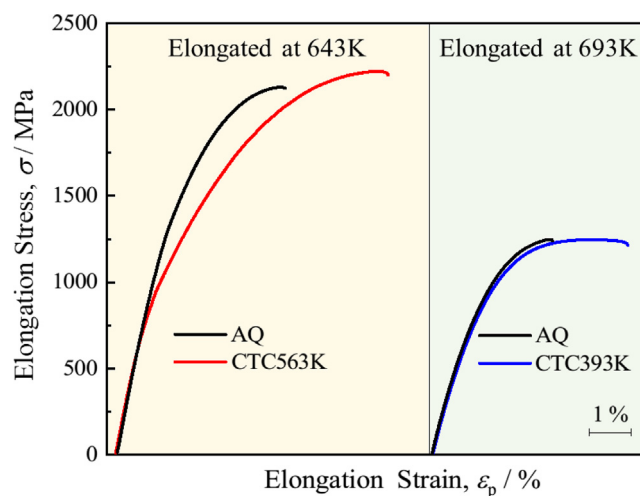


Fig. 3. The representative tensile stress–strain curves of the AQ and CTC563K samples elongated at 643 K (left part), and the AQ and CTC393K samples elongated at 693 K (right part).

slight β -relaxation activation at this temperature, as can be seen in Fig. 2(b). For CTC393K and CTC563K samples, the decreased σ_y and increased ε_p compared to AQ sample at corresponding temperatures indicate that more soft regions are involved in the two samples.

Fig. 4 shows the surfaces of CTC563K, CTC393K and AQ samples after tensile fracture at 643 and 693 K, respectively, and the insets show the vertical section morphologies. For CTC563K and CTC393K samples, multiple SBs are generated during tension, which proves that the deformation is not homogeneous but localized, and the intersections of multiple SBs may be responsible for the enhanced plastic deformation ability of the two samples. While for AQ sample, parallel SBs are dominated and the number of secondary SBs is smaller, this is consistent with the inferior plastic strain of AQ sample. The vertical section morphologies of these samples are also quite different, for CTC563K sample elongated at 643 K, the vertical section is flat and almost featureless shear plane, as can be seen in Fig. 4(a). No morphology related to liquid-like behavior is observed, which means the stable propagation of SBs [29]. For CTC393K sample elongated at 693 K, smooth shear offset, vein patterns along with many discontinuous floccules can be observed on

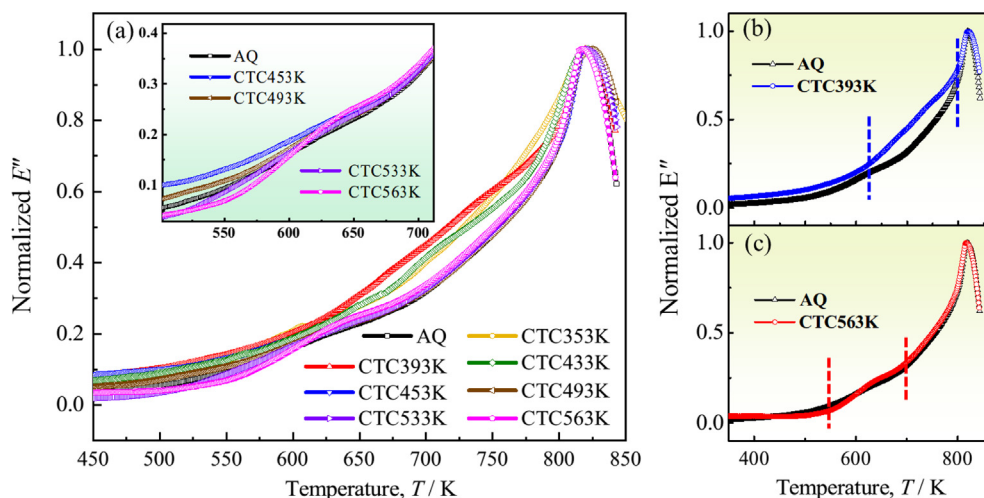


Fig. 2. The temperature dependence of the normalized loss modulus E'' for (a) the AQ and CTC treated MG ribbons, the inset is the enlarged image of part of the curves, (b) AQ and CTC393K samples, (c) AQ and CTC563K samples.

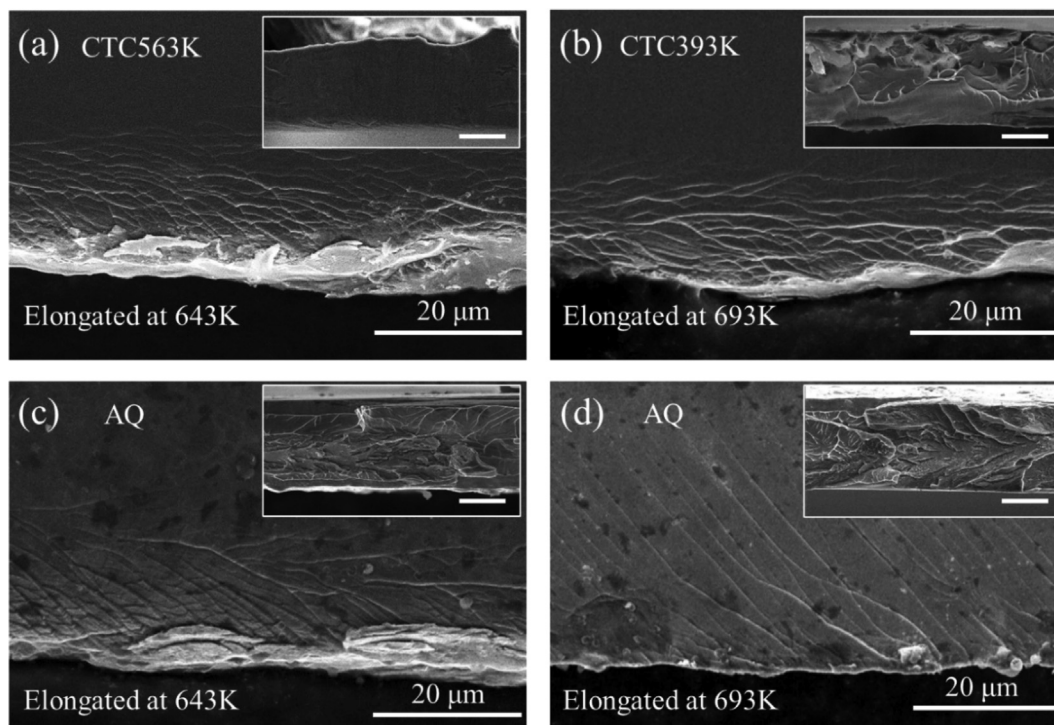


Fig. 4. The SEM images of the surfaces after tensile fracture for (a) the CTC563K sample elongated at 643 K, (b) the CTC393K sample elongated at 693 K, and AQ sample elongated at (c) 643 K and (d) 693 K. Insets show the SEM images of the vertical sections (scale bars – 10 μm).

the vertical section. These characters indicate the stable propagation of SBs at the beginning of deformation process, and the subsequent meniscus instability leading to a relatively fast propagation of SBs [30]. For AQ sample elongated at 643 K and 693 K (inset of Fig. 4(c) and Fig. 4(d)), cleavage features with ridges and rivers are observed [28], revealing the brittle fracture mechanism.

3.2. Energy states before and after thermal cycling

Fig. 5 shows the representative relaxation spectra and ΔH_{rel} with error bars of AQ and CTC treated samples. The ΔH_{rel} increases firstly and then decreases with incremental cycling temperature. The ΔH_{rel} of CTC393K sample is the largest, and for CTC533K and CTC563K samples, the ΔH_{rel} are much smaller than that of AQ sample. In general, the exothermic heat of relaxation is associated with

energy state and closely related to total fraction of free volume in MGs [31], a higher ΔH_{rel} often corresponds to more rejuvenated state and larger amount of free volumes [15,17,19]. However, actual structural relaxation may occur through not only the annihilation of free volume but also the annihilation of anti-free volume [32]. The anti-free volume with high energy state induced by local residual pressure has been reported in MGs after pressurized annealing [33] and CTC treatment [34]. According to this view, the total ΔH_{rel} change due to structural relaxation is the sum of two opposite contributions: the free volume part related to regions of low density, and the anti-free volume part related to regions of high density [35]. The decreased ΔH_{rel} of CTC533K and CTC563K samples may not reflect the real change of free volume and needs further exploration. In addition, it is worth noting that the change of ΔH_{rel} with cycling temperature in this work is quite different

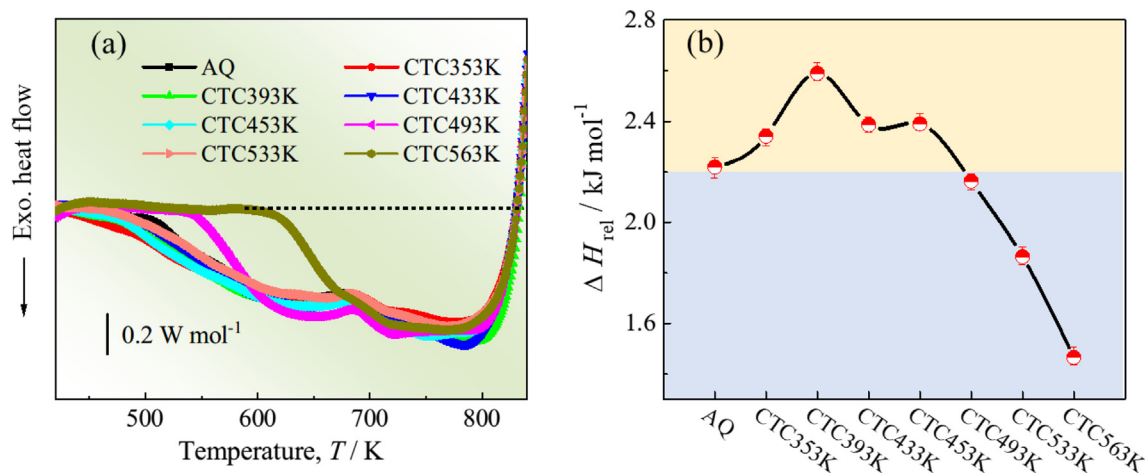


Fig. 5. The relaxation heat for the AQ and CTC treated MG ribbons. (a) The typical relaxation spectra, (b) the variation of ΔH_{rel} with error bars.

from the previous work with the same composition but in a bulk form [22]. This is because that the rejuvenation and relaxation process is caused by local stress during thermal cycling, the more disordered and heterogeneous structure of ribbons can help inducing larger local stress because of the wide differences of thermal expansion coefficient among different regions, so that the rejuvenation can be achieved at lower cycling temperature in ribbon samples. Besides, the atoms with high energy states in ribbon sample are more unstable and have higher mobility, thus the ribbon sample has a more tendency to be relaxed when the cycling temperature is higher.

3.3. Structure characterization

Figs. 6(a-c) are the HRTEM images of the AQ, CTC393K and CTC563K samples, with the selected area electron diffraction (SAED) patterns shown in the insets. The maze-like feature in the HRTEM micrograph together with the diffuse halo rings in SAED patterns suggest the amorphous structure before and after thermal cycling. However, the CTC treatment has a significant effect on the nanoscale structure. In the three samples, crystal-like ordered packing clusters of ~ 1 nm are found dispersed in the matrix, indicated by the white lines. These crystal-like orderings (CLOs) are confirmed to be pregnant structure of Fe_{23}B_6 phase, which is inclined to precipitate first in the (Fe,Co)-B-Si-Nb system [22]. In order to quantitatively analyze the orderings, 2D autocorrelation function analysis is utilized. Randomly selected regions of the HRTEM images of the three samples are divided into 100 square sub-cells with a size of $1.073 \text{ nm} \times 1.073 \text{ nm}$, which is close to the size of CLO structure, and the resulting images are shown in Figs. 6(d-f). The total fraction of CLO structures is 11% in AQ sample, 5% in CTC393K sample and 11% in CTC563K sample. It seems that the lower cycling temperature destroys part of the CLO structures, while the higher cycling temperature facilitates the forma-

tion of CLO structures. These phenomena have been reported before [22,36] and can be easily understood since the material is situated in dynamic energy changes of relaxation and rejuvenation. Combined with the ΔH_{rel} results, the CTC393K sample has a more disordered structure while the CTC563K sample tends to be more ordered after thermal cycling.

To explore the possible chemical or density fluctuations in nanoscale, high-resolution HAADF-TEM measurement is performed. The three samples show contrast with dark and bright areas in Figs. 7(a-c), as a result of inhomogeneous distributions of density and/or chemistry. The mappings of elements (Figs. 7(d-f)) of three samples show homogeneous distributions, and no visible chemical fluctuations are detected. Thus, the dark-bright contrasts in HAADF images mainly arise from the density variations. It is obvious that the inhomogeneous contrast increases for CTC393K and CTC563K samples, with more dark areas embedded, which is indicative of more inhomogeneous microstructure after thermal cycling. According to the previous nano-beam electron diffraction observation, the bright regions in the HAADF image have a relatively higher density and structure ordering, which correspond to the matrix. In contrast, the dark regions have a lower density and structure ordering, corresponding to the loosely packed regions [37]. These results indicate that the thermal cycling can promote atomic arrangements to an inhomogeneous configuration with more soft regions.

4. Discussion

The β -relaxation peaks and tensile plasticity are closely related to the STZs activation in MGs, the investigation on variation of STZ volume after thermal cycling makes great sense. Nanoindentation loading causes the activation and subsequent evolution of STZs in the shearing events, thus can connect the internal defects with external mechanical properties in MGs [38,39]. The activation vol-

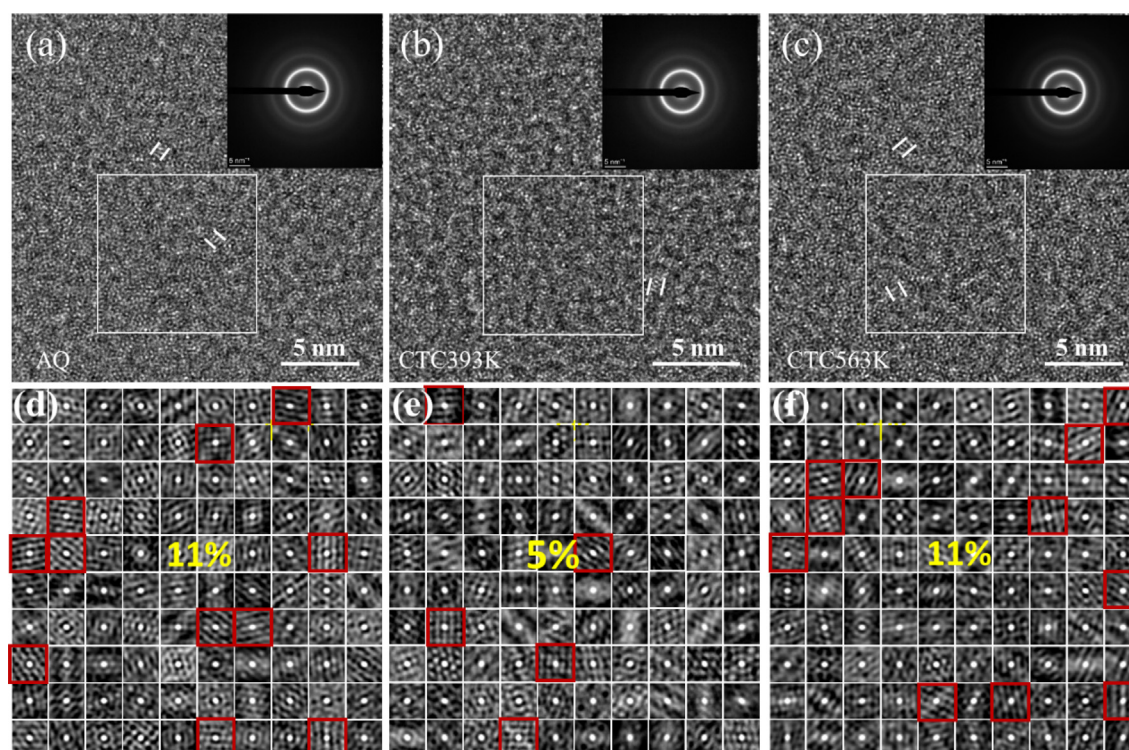


Fig. 6. The HRTEM images with corresponding SAED patterns as insets of (a) AQ, (b) CTC393K, and (c) CTC563K MG samples. The white lines highlight the CLO structures. (d-f) The 2D autocorrelation function analysis of the white square in (a-c), respectively.

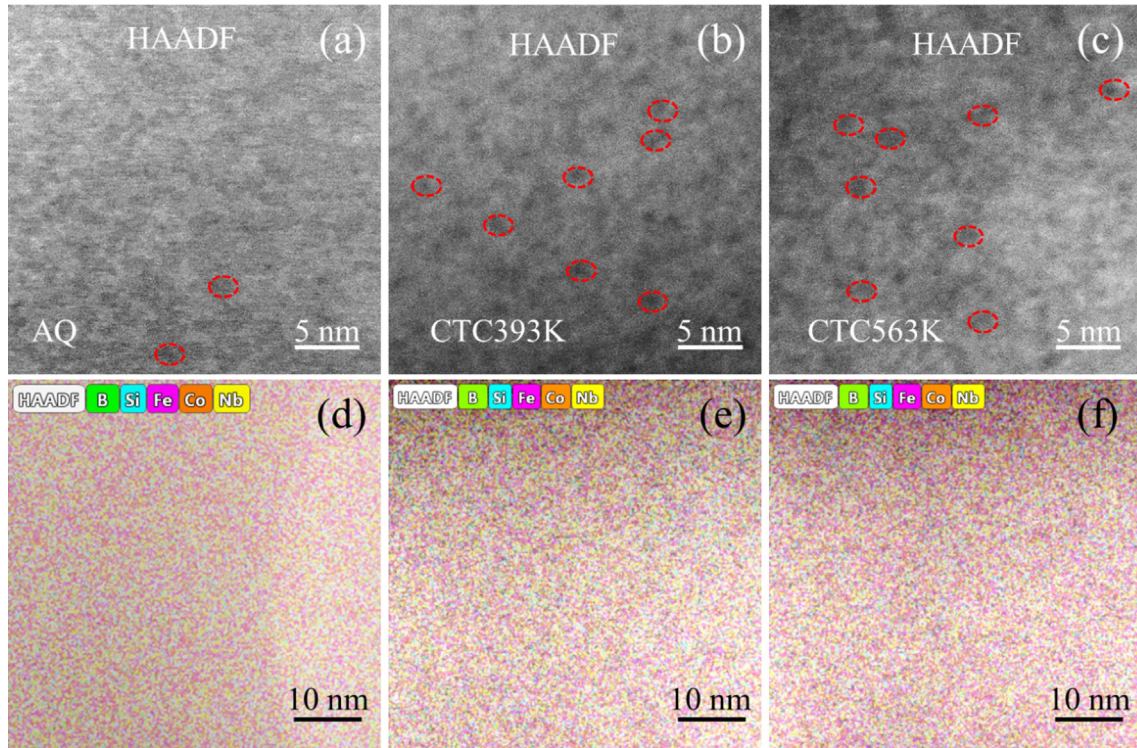


Fig. 7. (a-c) HAADF-HRTEM images and (d-f) the corresponding element mappings of AQ, CTC393K and CTC563K samples.

umes of STZ, Ω , of AQ, CTC393K and CTC563K samples are calculated based on the cooperative shear model (CSM) [27]:

$$\Omega = \frac{\tau_c \sqrt{3} k_B T}{2mHR\xi G_0 \gamma_c^2 (1 - \tau_{CT}/\tau_{CO})^{1/2}} \quad (1)$$

where k_B is the Boltzmann constant, T is the temperature and H is hardness. τ_c and G_0 are threshold shear resistance and shear modulus at 0 K, $\tau_{CT}/G_0 = 0.036$. The constants of R , ξ and γ_c are equal to 0.25, 3 and 0.027, respectively. The value of τ_{CT}/τ_{CO} at a certain T can be estimated by the following equation:

$$\tau_{CT}/\tau_{CO} = \frac{\gamma_{CO} - \gamma_{C1} (T/T_g)^{2/3}}{\tau_c/G_0} \quad (2)$$

the value of γ_{CO} is 0.036 ± 0.002 , γ_{C1} is 0.016 ± 0.002 .

Besides, m is the non-dimensional strain rate sensitivity index, derived by [38]:

$$m = \partial \ln H / \partial \ln \dot{\epsilon} \quad (3)$$

where $\dot{\epsilon}$ is the equivalent strain rate, derived by:

$$\dot{\epsilon} = \dot{P}/2P \quad (4)$$

P is the applied force, $\dot{P} = dP/dt$.

Four different strain rates of 0.5, 1, 5, and 10 mN/s were applied in the nanoindentation tests and Fig. 8 shows the critical parameter m in determining the STZ volumes. The values of m for AQ, CTC393K and CTC563K samples are 0.0167, 0.0128 and 0.0146, respectively. The activation volume is thus calculated to be 2.41 nm^3 for AQ, 3.16 nm^3 for CTC393K, and 2.66 nm^3 for CTC563K samples according to Eq. (1). Based on the CSM, the potential energy barrier W for an unsheared STZ is in proportion to Ω [27]. Thus, the CTC393K sample has the largest activation energy of STZ, while the variation of W is not such obvious for CTC563K sample compared with AQ sample. According to the previous finding, the potential energy barrier for STZ represents a linear fit with that

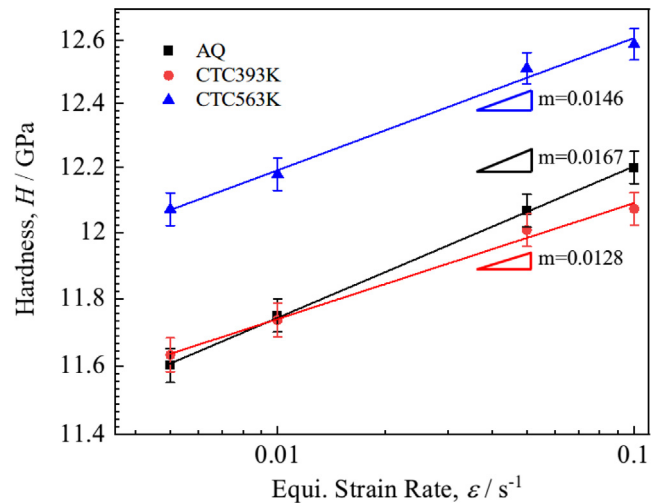


Fig. 8. Determination of the strain rate sensitivity m of AQ, CTC393K and CTC563K samples.

of β -relaxation in various MG systems [25]. Since the energy barrier of STZ is largest in CTC393K sample, it has the largest energy barrier of β -relaxation, which may illustrate the shift of β -relaxation to elevated temperature. For CTC563K sample, the energy barrier of β -relaxation seems to be similar with AQ sample, so as the position of β -relaxation peak. The striking phenomenon is that although the thermal temperatures range from 353 to 563 K and it seems that different thermal temperatures can lead to different STZ activation volumes, the β -relaxation peaks only appear at two separate temperatures. This maybe illustrated by the concept of atomically quantized hierarchy of STZs. M. Atzmon et al. studied the anelastic relaxation behavior of $\text{Al}_{86.8}\text{Ni}_{3.7}\text{Y}_{9.5}$ MG and found that the relaxation-time spectra exhibit a series of distinct peaks,

each spectrum peak is attributed to distinct STZ properties that differ from each other by one atomic volume, each STZ type has characteristic relaxation time constant [40,41]. Some studies believe that the system with insignificant β -relaxation is due to the large difference in the sizes of loosely arranged regions and the STZ, the β -relaxation cannot be activated intensively during the activation process [42]. The conspicuous β -relaxation of $[(\text{Fe}_{0.5}\text{Co}_{0.5})_{0.75}\text{B}_{0.2}\text{Si}_{0.05}]_{96}\text{Nb}_4$ MG indicates that there exists dominate size of loosely arranged regions. Since the β -relaxation peaks appear at two separate temperature regions, the activation volume of the dominate STZ is limited to two specific values.

In addition, Fig. 8 demonstrates that the average hardness differs a lot among the three samples. The CTC393K sample shows smaller hardness while the CTC563K sample shows much larger hardness compared to AQ sample. Combined with the ΔH_{rel} and HRTEM results, the CTC393K sample is well rejuvenated with more soft spots and loosely packed elastic surroundings, while the CTC563K sample is supposed to possess a densely packed matrix and local areas with certain numbers of anti-free volumes. Although CTC treatment is initially aimed at rejuvenation of MGs, various works have shown that this method can also induce relaxation or crystallization behavior [36,43]. Since the onset temperature of relaxation is around 500 K for the MG ribbons (suggested by the DSC curve of AQ sample, as can be seen in Fig. 5(a)), the thermal temperature of 563 K may result in relaxation to the MG. However, according to the HAADF results, rejuvenation happens simultaneously in local regions, bringing about areas with high energy states in CTC563K sample. The dominate size of loosely packed regions may be decreased compared to the CTC393K sample by the higher thermal temperature, resulting in a lower activation energy of dominate STZ and β -relaxation for CTC563K sample.

Based on the above analysis, the pronounced β -relaxation peak and enhanced tensile plasticity of CTC treated samples can be interpreted by considering the change of energy states and structural heterogeneities, which maybe originated from the change of distribution of atomic-level stress induced by thermal cycling [44]. During the process of CTC treatment, inhomogeneous contraction and expansion will introduce complex thermal stresses in the MG. The compressive stress facilitates the coalescence of soft spots and the elastic surroundings, and perhaps the formation of some denser areas with anti-free volumes [34,45]. While the tensile stress promotes the expansion of soft zones and the surrounding matrix. The magnitude of stress mainly depends on the temperature differences between 77 K and oil temperatures. However, due to the complexity of the structure and energy states of MGs, the final states of local atoms may be difficult to predict [36,43,45]. In this study, when the thermal temperature is lower, for instance, in CTC393K sample, more free volumes with high energy state are generated, resulted from the increase in quantity or volume of loosely packed regions. Under loading, the sample with abundant soft regions has a large inclination to execute a cascading activation of multiple STZs. Besides, the increased soft heterogeneities can transform the uniaxial stress field into a multi-axial complex stress field around STZs [46]. This slows the percolation process of STZ and thus the formation of critical SBs, delaying the shear failure. When the thermal temperature is higher, for example, in CTC563K sample, rejuvenation and relaxation occur simultaneously. The structure becomes more heterogeneous on account of increased number of loosely packed regions, dense matrix and much more densely packed areas with anti-free volumes. The regions with high anti-free volumes are unstable and rejuvenated with high energy state, thus are fertile sites for shear flow. It was reported that these denser areas have priority to be activated upon loading [34,47]. When the denser areas with anti-free volumes cannot bear more strain, it will subsequently trigger excitation of local STZ events. During the activation process

of STZs and SBs, the inhomogeneous hard and soft structures of CTC563K sample can also promote plastic deformation. In heterogeneous MG samples, the STZ-vortex mechanism is expected to be perturbed at the interface between the heterogeneities, the different characteristics at the two sides of the interface can perturb the percolation of STZs [48]. Besides, the stress distribution through the heterostructure changes significantly at the interface, not only perturbs the strain distribution but also changes its direction, facilitating the branching of SBs [46,48]. The extensive SB nucleation and bifurcation enable the shear deformation to be distributed among a large number of SBs, leading to the suppression of the onset of crack. Larger numbers of SBs, with each carrying relatively small amount of strains, are highly desirable for achieving large plasticity in MGs. As a result, although the CTC563K sample has less free volumes, the increased structural heterogeneity brings about enhanced tensile plasticity. Since the β -relaxation may share identical microstructural origins with STZ, the easier activation of multiple STZs in CTC393K and CTC563K samples contributes to the conspicuous β -relaxation behavior.

Previous work revealed that annealing treatment could remarkably reduce the amount of free volumes in loosely packed regions but hardly affect the intrinsic open-volume defects [49], leading to reduced intensity of β -relaxation peaks or humps in MGs [50]. Unlike annealing, thermal cycling allows for an effective manipulation of free volumes both in elastic matrix and loosely packed regions. Both the matrix and soft regions participate in dynamic relaxation and rejuvenation processes, the thermal cycling can impact on defects in soft regions and elastic matrix simultaneously, which makes it a powerful means of structure modification for MGs.

5. Conclusions

The $[(\text{Fe}_{0.5}\text{Co}_{0.5})_{0.75}\text{B}_{0.2}\text{Si}_{0.05}]_{96}\text{Nb}_4$ MG ribbons were treated with thermal cycling at different thermal temperatures. Pronounced β -relaxation was observed after CTC treatment, and the β -relaxation peaks appeared at two different positions, 550–700 K and 620–790 K. The CTC563K and CTC393K samples, which exhibited most remarkable β -relaxation at respective temperatures, showed tensile plastic strains of 5.2% at 643 K and 4.0% at 693 K. The tensile plastic strains for AQ sample at 643 and 693 K were only 3.0% and 2.1%, respectively. The enhanced tensile plasticity after CTC treatment is considered to be originated from the increased structural heterogeneity. It is worth noting that even though CTC is initially aimed at rejuvenation of MGs, it can also induce relaxation and oscillatory (rejuvenation-relaxation) behavior once the thermal temperature exceeds a certain limit. The contradictory behavior that the densification of elastic matrix as well as the increasing of loosely packed regions can be induced simultaneously. In addition, such oscillation also causes the variation of size of dominate STZ, which is responsible for the different positions of β -relaxation peak. These results not only provide a deep understanding of the structure changes during CTC treatment of Fe-based MGs, but also offer significant insights for designing and processing MGs with excellent mechanical properties.

Data availability

Data will be made available on request.

Declaration of Competing Interest

The authors declare that they have no known competing financial interests or personal relationships that could have appeared to influence the work reported in this paper.

Acknowledgments

This work was supported by the National Natural Science Foundation of China (Grant Nos. 51631003, 52071222), the Jiangsu Provincial Key Research and Development Program (Grant Nos. BE2021088), and the Guangdong Major Project of Basic and Applied Basic Research, China (Grant No. 2019B030302010).

References

- Y. Yoshizawa, S. Oguma, K. Yamauchi, New Fe-based soft magnetic alloys composed of ultrafine grain structure, *J. Appl. Phys.* 64 (1988) 6044–6046, <https://doi.org/10.1063/1.342149>.
- A. Inoue, B.L. Shen, C.T. Chang, Super-high strength of over 4000 MPa for Fe-based bulk glassy alloys in [(Fe_{1-x}Co_x)_{0.75}B_{0.2}Si_{0.05}]₉₆Nb₄ system, *Acta Mater.* 52 (2004) 4093–4099, <https://doi.org/10.1016/j.actamat.2004.05.022>.
- C. Suryanarayana, A. Inoue, Iron-based bulk metallic glasses, *Int. Mater. Rev.* 58 (2013) 131–166, <https://doi.org/10.1179/1743280412Y.0000000007>.
- Y. Wu, H.X. Li, Z.B. Jiao, J.E. Gao, Z.P. Lu, Size effects on the compressive deformation behaviour of a brittle Fe-based bulk metallic glass, *Philos. Mag. Lett.* 90 (2010) 403–412, <https://doi.org/10.1080/09500831003705344>.
- H. Bei, S. Xie, E.P. George, Softening caused by profuse shear banding in a bulk metallic glass, *Phys. Rev. Lett.* 96 (2006), <https://doi.org/10.1103/PhysRevLett.96.105503>.
- W.H. Jiang, F.X. Liu, P.K. Liaw, H. Choo, Shear strain in a shear band of a bulk-metallic glass in compression, *Appl. Phys. Lett.* 90 (2007), <https://doi.org/10.1063/1.2734502> 181903.
- C. Liu, Z. Cai, X. Xia, V. Roddatis, R. Yuan, J.M. Zuo, R. Maaß, Shear-band structure and chemistry in a Zr-based metallic glass probed with nano-beam x-ray fluorescence and transmission electron microscopy, *Scripta Mater.* 169 (2019) 23–27, <https://doi.org/10.1016/j.scriptamat.2019.05.005>.
- Z.F. Zhang, J. Eckert, L. Schultz, Difference in compressive and tensile fracture mechanisms of Zr₅₉Cu₂₀Al₁₀Ni₈Ti₃ bulk metallic glass, *Acta Mater.* 51 (2003) 1167–1179, [https://doi.org/10.1016/S1359-6454\(02\)00521-9](https://doi.org/10.1016/S1359-6454(02)00521-9).
- W.M. Yang, H.S. Liu, Y.C. Zhao, A. Inoue, K.M. Jiang, J.T. Huo, H.B. Ling, Q. Li, B.L. Shen, Mechanical properties and structural features of novel Fe-based bulk metallic glasses with unprecedented plasticity, *Sci. Rep.* 4 (2014) 6233, <https://doi.org/10.1038/srep06233>.
- S.F. Guo, J.L. Qiu, P. Yu, S.H. Xie, W. Chen, Fe-based bulk metallic glasses: Brittle or ductile?, *Appl. Phys. Lett.* 105 (16) (2014) 161901, <https://doi.org/10.1063/1.4899124>.
- J. Zhou, Q.Q. Wang, X.D. Hui, Q.S. Zeng, Y.W. Xiong, K.B. Yin, B.A. Sun, L.T. Sun, M. Stoica, W.H. Wang, B.L. Shen, A novel FeNi-based bulk metallic glass with high notch toughness over 70 MPa m^{1/2} combined with excellent soft magnetic properties, *Mater. Des.* 191 (2020), <https://doi.org/10.1016/j.matdes.2020.108597> 108597.
- B. Sarac, Y.P. Ivanov, A. Chuvilin, T. Schöberl, M. Stoica, Z.L. Zhang, J. Eckert, Origin of large plasticity and multiscale effects in iron-based metallic glasses, *Nat. Commun.* 9 (2018) 1333, <https://doi.org/10.1038/s41467-018-03744-5>.
- S.F. Guo, L. Liu, N. Li, Y. Li, Fe-based bulk metallic glass matrix composite with large plasticity, *Scripta Mater.* 62 (2010) 329–332, <https://doi.org/10.1016/j.scriptamat.2009.10.024>.
- A. Makino, X. Li, K. Yubuta, C.T. Chang, T. Kubota, A. Inoue, The effect of Cu on the plasticity of Fe-Si-B-P-based bulk metallic glass, *Scripta Mater.* 60 (2009) 277–280, <https://doi.org/10.1016/j.scriptamat.2008.09.008>.
- J. Pan, Y.P. Ivanov, W.H. Zhou, Y. Li, A.L. Greer, Strain-hardening and suppression of shear-banding in rejuvenated bulk metallic glass, *Nature* 578 (2020) 559–562, <https://doi.org/10.1038/s41586-020-2016-3>.
- L. Zhao, K.C. Chan, S.H. Chen, S.D. Feng, D.X. Han, G. Wang, Tunable tensile ductility of metallic glasses with partially rejuvenated amorphous structures, *Acta Mater.* 169 (2019) 122–134, <https://doi.org/10.1016/j.actamat.2019.03.007>.
- S.V. Ketov, Y.H. Sun, S. Nachum, Z. Lu, A. Checchi, A.R. Beraldin, H.Y. Bai, W.H. Wang, D.V. Louzguine-Luzgin, M.A. Carpenter, A.L. Greer, Rejuvenation of metallic glasses by non-affine thermal strain, *Nature* 524 (2015) 200–203, <https://doi.org/10.1038/nature14674>.
- B.S. Li, S.H. Xie, J.J. Kruzic, Toughness enhancement and heterogeneous softening of a cryogenically cycled Zr-Cu-Ni-Al-Nb bulk metallic glass, *Acta Mater.* 176 (2019) 278–288, <https://doi.org/10.1016/j.actamat.2019.07.012>.
- W.L. Song, X.H. Meng, Y. Wu, D. Cao, H. Wang, X.J. Liu, X.Z. Wang, Z.P. Lu, Improving plasticity of the Zr₄₆Cu₄₆Al₈ bulk metallic glass via thermal rejuvenation, *Sci. Bull.* 63 (2018) 840–844, <https://doi.org/10.1016/j.scib.2018.04.021>.
- H. Zheng, L. Zhu, S.S. Jiang, Y.G. Wang, F.G. Chen, Recovering the bending ductility of the stress-relieved Fe-based amorphous alloy ribbons by cryogenic thermal cycling, *J. Alloys Compd.* 790 (2019) 529–535, <https://doi.org/10.1016/j.jallcom.2019.03.213>.
- S.V. Ketov, A.S. Trifonov, Y.P. Ivanov, A.Y. Churyumov, A.V. Lubchenko, A.A. Batrakov, J. Jiang, D.V. Louzguine-Luzgin, J. Eckert, J. Orava, A.L. Greer, On cryothermal cycling as a method for inducing structural changes in metallic glasses, *NPG Asia Mater.* 10 (2018) 137–145, <https://doi.org/10.1038/s41427-018-0019-4>.
- S.Y. Di, Q.Q. Wang, J. Zhou, Y.Y. Shen, J.Q. Li, M.Y. Zhu, K.B. Yin, Q.S. Zeng, L.T. Sun, B.L. Shen, Enhancement of plasticity for FeCoBSiNb bulk metallic glass with superhigh strength through cryogenic thermal cycling, *Scripta Mater.* 187 (2020) 13–18, <https://doi.org/10.1016/j.scriptamat.2020.05.059>.
- J. Ketkaew, R. Yamada, H. Wang, D. Kuldinov, B.S. Schroers, W. Drnowski, T. Egami, J. Schroers, The effect of thermal cycling on the fracture toughness of metallic glasses, *Acta Mater.* 184 (2020) 100–108, <https://doi.org/10.1016/j.actamat.2019.11.046>.
- B.S. Shang, W.H. Wang, A.L. Greer, P.F. Guan, Atomistic modelling of thermal-cycling rejuvenation in metallic glasses, *Acta Mater.* 213 (2021), <https://doi.org/10.1016/j.actamat.2021.116952> 116952.
- H.B. Yu, W.H. Wang, H.Y. Bai, Y. Wu, M.W. Chen, Relating activation of shear transformation zones to beta relaxations in metallic glasses, *Phys. Rev. B* 81 (2010), <https://doi.org/10.1103/PhysRevB.81.220201> 220201.
- H.B. Yu, X. Shen, Z. Wang, L. Gu, W.H. Wang, H.Y. Bai, Tensile plasticity in metallic glasses with pronounced beta relaxations, *Phys. Rev. Lett.* 108 (2012), <https://doi.org/10.1103/PhysRevLett.108.015504> 015504.
- W.L. Johnson, K. Samwer, A universal criterion for plastic yielding of metallic glasses with a (T/T_g)^{2/3} temperature dependence, *Phys. Rev. Lett.* 95 (2005), <https://doi.org/10.1103/PhysRevLett.95.195501> 195501.
- G. Wang, J. Shen, J.F. Sun, Z.P. Lu, Z.H. Stachurski, B.D. Zhou, Tensile fracture characteristics and deformation behavior of a Zr-based bulk metallic glass at high temperatures, *Intermetallics* 13 (2005) 642–648, <https://doi.org/10.1016/j.intermet.2004.10.011>.
- D.T.A. Matthews, V. Ocelik, P.M. Bronsveld, J.T.M. De Hosson, An electron microscopy appraisal of tensile fracture in metallic glasses, *Acta Mater.* 56 (2008) 1762–1773, <https://doi.org/10.1016/j.actamat.2007.12.029>.
- Z.C. Ma, H.W. Zhao, X.J. Du, X.X. Ma, Z.F. Qiang, F. Zhang, L.M. Zhou, L.Q. Ren, Static and cyclic mechanical behaviours and fracture mechanisms of Zr-based metallic glass at elevated temperatures, *Philos. Mag.* 99 (2019) 835–852, <https://doi.org/10.1080/14786435.2018.1562280>.
- L.Y. Chen, A.D. Setyawan, H. Kato, A. Inoue, G.Q. Zhang, J. Saida, X.D. Wang, Q.P. Cao, J.Z. Jiang, Free-volume-induced enhancement of plasticity in a monolithic bulk metallic glass at room temperature, *Scripta Mater.* 59 (2008) 75–78, <https://doi.org/10.1016/j.scriptamat.2008.02.025>.
- D.B. Miracle, T. Egami, K.M. Flores, K.F. Kelton, Structure aspects of metallic glasses, *MRS Bull.* 32 (2007) 629–634, <https://doi.org/10.1557/mrs2007.124>.
- A. Foroughi, H. Ashuri, R. Tavakoli, M. Stoica, D. Şopu, J. Eckert, Structural modification through pressurized sub-T_g annealing of metallic glasses, *J. Appl. Phys.* 122 (2017), <https://doi.org/10.1063/1.5004058> 215106.
- N.Z. Zhang, X.L. Bian, C. Ren, C. Geng, Y.K. Mu, X.D. Ma, Y.D. Jia, Q. Wang, G. Wang, Manipulation of relaxation processes in a metallic glass through cryogenic treatment, *J. Alloys Compd.* 894 (2022), <https://doi.org/10.1016/j.jallcom.2021.162407> 162407.
- S. Scudino, M. Stoica, I. Kaban, K.G. Prashanth, G.B.M. Vaughan, J. Eckert, Length scale-dependent structural relaxation in Zr_{57.5}Ti_{7.5}Nb₅Cu_{12.5}Ni₁₀Al_{7.5} metallic glass, *J. Alloys Compd.* 639 (2015) 465–469, <https://doi.org/10.1016/j.jallcom.2015.03.179>.
- S.Y. Di, Q.Q. Wang, Y.Y. Yang, T. Liang, J. Zhou, L. Su, K.B. Yin, Q.S. Zeng, L.T. Sun, B.L. Shen, Efficient rejuvenation of heterogeneous [(Fe_{0.5}Co_{0.5})_{0.75}B_{0.2}Si_{0.05}]₉₆Nb₄ bulk metallic glass upon cryogenic cycling treatment, *J. Mater. Sci. Technol.* 97 (2022) 20–28, <https://doi.org/10.1016/j.jmst.2021.04.034>.
- F. Zhu, A. Hirata, P. Liu, S.X. Song, Y. Tian, J.H. Han, T. Fujita, M.W. Chen, Correlation between local structure order and spatial heterogeneity in a metallic glass, *Phys. Rev. Lett.* 119 (2017), <https://doi.org/10.1103/PhysRevLett.119.215501> 215501.
- D. Pan, A. Inoue, T. Sakurai, M.W. Chen, Experimental characterization of shear transformation zones for plastic flow of bulk metallic glasses, *Proc. Natl. Acad. Sci.* 105 (2008) 14769–14772, <https://doi.org/10.1073/pnas.0806051105>.
- H. Guo, C.B. Jiang, B.J. Yang, J.Q. Wang, Deformation behavior of Al-rich metallic glasses under nanoindentation, *J. Mater. Sci. Technol.* 33 (2017) 1272–1277, <https://doi.org/10.1016/j.jmst.2016.10.014>.
- J.D. Ju, D. Jang, A. Nwankpa, M. Atzmon, An atomically quantized hierarchy of shear transformation zones in a metallic glass, *J. Appl. Phys.* 109 (2011), <https://doi.org/10.1063/1.3552300> 053522.
- T.J. Lei, L.R. DaCosta, M. Liu, J. Shen, Y.H. Sun, W.H. Wang, M. Atzmon, Composition dependence of metallic glass plasticity and its prediction from anelastic relaxation-A shear transformation zone analysis, *Acta Mater.* 195 (2020) 81–86, <https://doi.org/10.1016/j.actamat.2020.04.053>.
- Z. Lu, B.S. Shang, Y.T. Sun, Z.G. Zhu, P.F. Guan, W.H. Wang, H.Y. Bai, Revealing β-relaxation mechanism based on energy distribution of flow units in metallic glass, *J. Chem. Phys.* 144 (2016), <https://doi.org/10.1063/1.4945279> 144501.
- W. Guo, J.J. Saida, M. Zhao, S.L. Lu, S.S. Wu, Non-thermal crystallization process in heterogeneous metallic glass upon deep cryogenic cycling treatment, *J. Mater. Sci.* 54 (2019) 8778–8785, <https://doi.org/10.1007/s10853-019-03515-7>.
- T. Egami, Atomic level stresses, *Prog. Mater. Sci.* 56 (2011) 637–653, <https://doi.org/10.1016/j.pmatsci.2011.01.004>.
- A. Das, E.M. Dufresne, R. Maaß, Structural dynamics and rejuvenation during cryogenic cycling in a Zr-based metallic glass, *Acta Mater.* 196 (2020) 723–732, <https://doi.org/10.1016/j.actamat.2020.06.063>.
- X.L. Bian, D. Şopu, G. Wang, B.A. Sun, J. Bednarčík, C. Gammer, Q.J. Zhai, J. Eckert, Signature of local stress states in the deformation behavior of metallic glasses, *NPG Asia Mater.* 12 (2020) 59, <https://doi.org/10.1038/s41427-020-00241-4>.

- [47] B. Wang, L.J. Wang, B.S. Shang, X.Q. Gao, Y. Yang, H.Y. Bai, M.X. Pan, W.H. Wang, P.F. Guan, Revealing the ultra-low-temperature relaxation peak in a model metallic glass, *Acta Mater.* 195 (2020) 611–620, <https://doi.org/10.1016/j.actamat.2020.05.067>.
- [48] D. Şopu, S. Scudino, X.L. Bian, C. Gammer, J. Eckert, Atomic-scale origin of shear band multiplication in heterogeneous metallic glasses, *Scripta Mater.* 178 (2020) 57–61, <https://doi.org/10.1016/j.scriptamat.2019.11.006>.
- [49] D. Suh, R.H. Dauskardt, P. Asoka-Kumar, P.A. Sterne, R.H. Howell, Temperature dependence of positron annihilation in a Zr-Ti-Ni-Cu-Be bulk metallic glass, *J. Mater. Res.* 18 (2003) 2021–2024, <https://doi.org/10.1557/JMR.2003.0283>.
- [50] R. Casalini, C.M. Roland, Aging of the secondary relaxation to probe structural relaxation in the glassy state, *Phys. Rev. Lett.* 102 (2009), <https://doi.org/10.1103/PhysRevLett.102.035701> 035701.